GLUT1 is redundant in hypoxic and glycolytic nucleus pulposus cells of the intervertebral disc

Shira N. Johnston[1,2,#], Elizabeth S. Silagi[1,2,3,#], Vedavathi Madhu[1], Irving M. Shapiro[1,2], Makarand V. Risbud[1,2,*]

[1]Department of Orthopaedic Surgery, Sidney Kimmel Medical College, Thomas Jefferson University, Philadelphia, PA, USA
[2]Graduate Program in Cell Biology and Regenerative Medicine, Jefferson College of Life Sciences, Thomas Jefferson University, Philadelphia, PA, USA
[3]Current affiliation - Department of Neurobiology, Harvard Medical School, Dana-Farber Cancer Institute, Boston, MA, USA

[#] Have contributed equally to this work

ABSTRACT

Glycolysis is central to homeostasis of nucleus pulposus (NP) cells in the avascular intervertebral disc. Since the glucose importer, GLUT1, is a well-established phenotypic marker of NP cells, we hypothesized that it is vital for development and post-natal maintenance of the disc. Surprisingly, primary NP cells treated with two well-characterized GLUT1 inhibitors maintained normal rates of glycolysis and ATP production, indicating intrinsic compensatory mechanisms. We show that NP cells mitigate the loss of GLUT1 function by rewiring glucose import through alternative transporters, particularly GLUT3 and possibly GLUT9/SGLT1, all of which are expressed in the disc. Noteworthy, we demonstrate that alternative substrates, such as glutamine and palmitate, do not compensate glucose restriction resulting from dual inhibition of GLUT1/3 by Glutor and inhibition compromises long-term cell viability. To investigate redundancy of GLUT1 function in NP *in vivo*, we generated two NP-specific knockout mice: Krt19^{CreERT}; Glut1$^{f/f}$ and Foxa2^{Cre}; Glut1$^{f/f}$. In contrast to the strong phenotype of tissue-specific Glut1 knockout mice in other connective tissues and supporting our *in vitro* findings, there were no apparent defects in post-natal disc maintenance (K19^{CreERT}; Glut1$^{f/f}$) or development and maturation (Foxa2^{Cre}; Glut1$^{f/f}$) in mutant mice. Microarray analysis confirmed that GLUT1 loss in the NP compartment did not cause transcriptomic alterations, supporting that NP cells are refractory to GLUT1 loss. These findings provide the first evidence of functional redundancy in GLUT transporters in the physiologically hypoxic intervertebral disc and underscore the importance of glucose as the indispensable metabolic substrate for NP cells.

SIGNIFICANCE STATEMENT

Glucose import into hypoxic nucleus pulposus cells is critical for maintaining glycolysis and intervertebral disc health. However, glucose import specifically through GLUT1, a highly enriched NP phenotypic marker, is surprisingly redundant. Another high capacity glucose transporter, GLUT3, appears sufficient to compensate for loss of GLUT1 function. Importantly, under glucose limiting conditions, NP cells do not switch to utilizing glutamine or fatty acid palmitate as metabolic substrates for mitochondrial oxidation. These findings underscore the necessity for built-in redundancy of glucose transporters in NP cells, where glucose is an indispensable metabolic substrate. This redundancy contrasts with the critical role that GLUT1 plays in the development and homeostasis of bone and cartilage.

INTRODUCTION

The phenotype of nucleus pulposus (NP) cells reflects their notochordal origin and unique hypoxic milieu[1–3]. One of the first attempts to define the NP cell phenotype identified that the HIF-1α transcription factor and glucose transporter, GLUT1, were highly enriched in the NP and not the annulus fibrosus (AF) compartment of the intervertebral disc [4]. NP cells constitutively express HIF-1α to facilitate hypoxic adaptation, given that the vasculature in the adjacent vertebral bodies does not penetrate the NP compartment [5,6]. As such, HIF-1α facilitates the biosynthetic capacity of NP cells by regulating glycolytic metabolism and mitochondrial TCA cycle and conditional deletion of HIF-1α in notochord results in massive NP cell apoptosis at birth likely due to metabolic failure [7–9]. Further investigations into the HIF-1α transcriptional program showed that Glut1 was HIF-1 target and expression was regulated through PHD3 dependent modulation of HIF-1α-C-TAD activity [10].

It has been well established that the maintenance of glycolytic flux and nutrient-metabolite balance is critical for cell survival in the intervertebral disc. Glucose passively diffuses from the vertebral capillaries, through the hyaline cartilaginous endplates and proteoglycan-rich extracellular matrix of the NP tissue compartment to reach the resident NP cells at the center of the disc. Despite this distance, glucose levels must surpass a critical threshold for cells to remain viable; glucose concentrations below 0.5 mmol/L are shown to promote cell death [11]. Numerous studies have confirmed that glucose availability is required for critical NP cellular processes such as protein and proteoglycan biosynthesis, glycolytic flux, and maintaining cell viability [12–15].

Furthermore, disruption in the balance between glucose consumption and lactic acid production can significantly impact NP cell physiology [16,17]. Several factors can influence the rate of glucose consumption in NP cells, including nutrient deprivation from decreased glucose diffusivity or increased cell density [18]; pH buffering capacity governed by relative levels of bicarbonate and sodium [19]; mechanical stress [20], and oxygen tension [21,22].

Despite the well-studied importance of glucose availability and consumption on NP cell viability *in vitro*, few studies have elucidated the correlation between glucose consumption and disc degeneration *in vivo*. This is due to the complexity of studying solute transport and metabolite concentrations in animal models or by using genetic techniques. Studies have shown enriched expression of GLUT1 in human NP and that GLUT3 and GLUT9 levels were lower than GLUT1 [23]. These results suggest that GLUT1 expression may be required for health and maintenance of the intervertebral disc with age.

Considering that GLUT1 is a high affinity glucose transporter with nearly ubiquitous expression in all tissue types, it is not surprising that embryos with homozygous GLUT1 deficiency are nonviable [24]. GLUT1 haploinsufficiency in mice causes profound developmental defects recapitulating those seen in human patients with GLUT1 deficiency syndrome [25]. Both humans and mice with GLUT1 haploinsufficiency experience microcephaly, impaired motor function, epileptiform changes on EEG, and hypoglycorrhachia [25]. Due to the severe impact of loss of GLUT1 on gross embryonic development, researchers have generated tissue-specific knock-out mice to delineate the role of GLUT1 in skeletal and other connective tissues [26–30]. These studies show that GLUT1 deletion leads to metabolic reprogramming of cells, profound phenotypic changes, and compromised tissue function. Concerning skeleton, loss of GLUT1 expression results in severely impaired bone development, providing nuance to the relationship between bone and glucose metabolism. Specifically, it is shown that GLUT1 expression precedes Runx2, and is required for promoting bone formation by blocking AMPK-dependent degradation of Runx2 [27]. On the other hand, GLUT1 is also shown to be controlled by a unique BMP-mTORC1-HIF1 signaling cascade in chondrocytes where it is required for chondrocyte proliferation and hypertrophy [28]. Mouse models of *Glut1* loss of function in growth plate and articular cartilage demonstrate that *Glut1* function is required for cartilage homeostasis, particularly relating to cell proliferation, matrix production and resistance to injury and osteoarthritis [31].

Since GLUT1-mediated glycolytic metabolism plays a fundamental role in many tissues including bone and cartilage homeostasis, we surmised that loss of GLUT1 expression in the NP

would impact both disc development and age-related maintenance [26–30]. Contrary to other skeletal tissues, both conditional and inducible loss of GLUT1 expression in the NP did not instigate notable degenerative changes in the discs of developing perinatal mice or in skeletally mature mice. Surprisingly, microarray analysis of global transcriptomic changes in NP tissue isolated from conditional GLUT1 knock-out mice did not uncover any differentially regulated genes besides *Slc2a1* (encoding GLUT1) – a finding which suggests NP cells are refractory to loss of GLUT1. In fact, long-term GLUT1 inhibition had no effect on the rates of NP glycolytic flux or oxidative metabolism since NP cells potentially mitigate the loss of GLUT1 function by rewiring glucose import through GLUT3. Importantly, our findings suggest that under glucose limiting conditions resulting from dual inhibition of GLUT1/3, NP cells do not undergo metabolic reprogramming to use alternative substrates, such as glutamine and fatty acids. These findings provide the first evidence of functional redundancy in GLUT transporters in a physiologically hypoxic intervertebral disc and underscore the importance of glucose as the indispensable metabolic substrate for NP cells.

Results

GLUT1 expression is highly enriched in the NP, is HIF-1 dependent and declines with age

During embryogenesis, the notochord and developing nucleus pulposus (NP) compartment of the intervertebral disc is hypoxic and has robust HIF-1α activity. Our previous work has shown that notochord-specific HIF-1α deletion in Foxa2^{Cre}; HIF-1$\alpha^{f/f}$ (HIF-1α^{cKO}) mice leads to massive NP cell death at birth, likely due to metabolic failure of cells that rely primarily on glycolytic metabolism for their energetic needs [7–9]. It is therefore not surprising that through early development to skeletal maturity expression of glucose transporter, *Slc2a1* (GLUT1) is highly enriched in NP cells (Fig. 1a) and is regarded as a phenotypic marker [3,32,33]. In fact, GLUT1 expression is substantially decreased in the NP of E15.5 HIF-1α^{cKO} mice without affecting level of carbonic anhydrase 3 (CA3), another hypoxia sensitive NP-phenotypic marker [34] (Fig. 1b,b'). These results indicate that loss of GLUT1 and consequent restriction on glucose availability shortly precedes the catastrophic NP cell death observed in HIF-1α^{cKO} mice at birth. Furthermore, changes in GLUT1 expression in intervertebral disc has been correlated to both age and degeneration state [23]. Our studies show that in mice, GLUT1 expression is significantly decreased during normal aging from 1 month to 24 months (Fig. 1c-c', 1d). Immunofluorescence staining of

GLUT1 shows robust expression of GLUT1 in NP-compartment at early timepoints, followed by a significant decrease in GLUT1 abundance by 24 months of age (Fig. 1c-c'). In fact, Western blot confirmed that GLUT1 protein level was markedly decreased by as early as 14 months of age (Fig. 1d). Based on these findings we hypothesized that GLUT1 is critically important for NP cell survival and function.

Long-term inhibition of GLUT1 does not affect glycolytic or oxidative metabolism in NP cells

To determine if loss of GLUT1 function directly impairs NP cell metabolism, we modeled loss of GLUT1 in NP cells *in vitro* with two highly specific pharmacological inhibitors; namely, BAY-876 and WZB-117 [35,36]. Using a Seahorse Flux Analyzer, we assessed metrics of NP cell glycolytic flux by measuring Extracellular Acidification Rate (ECAR) and oxidative flux by oxygen consumption rate (OCR). After short-term inhibition of GLUT1 for 1 hour, NP cells showed significantly decreased average ECAR with both inhibitors (Fig. 1e, f, g). However, total OCR and mitochondrial OCR remained unchanged, suggesting the NP cells did not undergo a metabolic switch from glycolytic to oxidative metabolism (Fig. 1e', f', h, h'). Specifically, the lack of NP cell response to electron transport chain inhibition with Antimycin A implies that baseline mitochondrial respiration remains low in both control and GLUT1 loss-of-function conditions (Fig. 1e', f').

To understand whether longer-term inhibition of GLUT1 similarly affects NP cell metabolism, we measured ECAR, OCR, and calculated the ATP production rates from glycolysis and oxidative metabolism in NP cells treated with two concentrations of BAY-876 and WZB-117 for 24h. We recorded raw ECAR and OCR traces under basal conditions (no glucose), followed by sequential addition of glucose (substrate), oligomycin (ATP-synthase inhibitor), and rotenone + myxothiozol (ETC inhibitors) (Fig. 2a-b'). Surprisingly, there were no significant differences in the average ECAR and OCR between control and GLUT1-inhibited NP cells (Fig. 2c, d), as is also evident from the raw tracer profiles. Using the published method by Mookerjee and colleagues [37], we calculated glycolytic and oxidative ATP production rates following GLUT1 inhibition with BAY-876 and WZB-117. It is important to note that under basal conditions (no glucose), oxidative metabolism generates ~50% of ATP in control NP cells, however this decreases to ~10-25% when glucose is added (Fig. 2e, e'). Furthermore, blocking oxidative ATP production entirely with oligomycin showed strikingly little effect on glycolytic ATP production rate, suggesting that glycolytic flux is largely independent of oxidative metabolism in NP cells (Fig. 2e, e'). Importantly, our results showed that there was no difference in ATP production rates from

glycolysis or oxidative phosphorylation in GLUT1-inhibited cells as compared to controls (Fig. 2e, e'). Taken together, the results of the Seahorse metabolic assays suggested that inhibiting glucose uptake though GLUT1 in NP cells causes an immediate decrease in glycolytic flux. However, compensatory mechanisms are capable of restoring NP cell glycolytic metabolism within 24 hours, without initiating a metabolic shift towards oxidative metabolism.

GLUT3 sustains glucose uptake in absence of GLUT1

Although GLUT1 is the highest expressed transporter in the NP, other glucose transporters including hypoxia sensitive GLUT3 and GLUT9 reported to be expressed in NP may also facilitate glucose uptake [3,23]. To test this hypothesis, we evaluated if GLUT1 is solely required for glucose import by measuring glucose uptake in NP cells treated with GLUT1 inhibitors, BAY-876/WZB-117, and potent GLUT1/2/3 inhibitor, Glutor. We treated primary NP cells with the glucose mimic, 2-deoxyglucose (2-DG), and measured the subsequent intracellular accumulation of 2-deoxyglucose-6-phosphate, which cannot undergo glycolysis. The 2-DG uptake assay clearly showed that simultaneously blocking GLUT1 and GLUT3 decreased glucose uptake by up to 80 to 90% compared to control in a dose and time dependent manner (Fig. 3a, a'). Interestingly, GLUT1 inhibition alone for 6 and 24 hours with BAY-876 or WZB-117 did not result in decreased glucose uptake implying a rapid compensation of loss of GLUT1 function. These findings also suggests that alternative glucose transporters, such as GLUT3, as NP cells do not express GLUT2, compensate for GLUT1 and may be responsible for a considerable amount of glucose uptake in NP cells.

These results raised a possibility that simultaneous inhibition of GLUT1 and GLUT3 long-term will compromise NP cell survival. We therefore measured NP cell viability following Glutor treatment for up to 72 hours. It was evident that cell viability decreased with increasing Glutor dose and the time of treatment (Fig. 3b-b''). Moreover, similar to GLUT1, there was a robust decrease in GLUT3 levels in the NP of E15.5 HIF-1α^{cKO} mice suggesting that pronounced cell death observed at birth in the NP compartment of these cKO mice could be in part due to constrained availability of glucose aggravating metabolic failure [9] (Fig. 3c, S.Fig. 1).

NP cells do not switch to glutamine and fatty acid oxidation under glucose limiting conditions following GLUT1/3 inhibition

Since glucose is the major energy source for most cell types, blocking its availability will shift cellular metabolism towards other substrates such as glutamine and/or fatty acids to maintain

TCA cycle flux. Our previous studies have shown that although NP cells do not rely on oxidative phosphorylation for ATP production, the TCA cycle is intact and serves as a hub for generation of metabolic intermediates used in broad biosynthesis reactions. In recent years, TCA cycle intermediates have also been shown to “moonlight” in the nucleus where they engage in the epigenetic regulation of DNA and histone modifications [38].

To gain an insight into whether the significant loss of glucose import though GLUT1 and GLUT3 upregulates 1) glutamine metabolism or 2) fatty acid oxidation, we performed substrate dependent Seahorse experiments with glucose + glutamine or BSA-palmitate. To assess effects on glutamine metabolism, NP cells were treated with Glutor for 24 hours prior to Seahorse assessment. We analyzed raw OCR and ECAR traces beginning with endogenous conditions (no substrate), followed by the sequential addition of glucose + glutamine (basal), oligomycin (ATP synthase inhibitor), FCCP (oxidative phosphorylation uncoupler), and BPTES (glutaminase inhibitor) (Fig. 3d-d’’’). Glutor-treatment significantly decreased endogenous OCR and basal OCR in the presence of glucose and glutamine, implying glutamine oxidation alone is not sufficient to rescue OCR in NP cells (Fig. 3d’’). Subsequently, control and Glutor-treated NP cells showed an expected decrease in OCR with oligomycin treatment, however FCCP was unable to shift 250 nM Glutor-treated cells to maximal OCR regardless of glutamine availability (Fig. 3d’’). To determine the contribution of glutamine oxidation, we inhibited glutaminase with BPTES. Interestingly, BPTES treatment did not decrease OCR in the control group suggesting that NP cells do not prefer glutamine oxidation in presence of glucose. Importantly, taken together this data suggested that blocking glucose import through GLUT1/3 inhibition did not result in increased glutamine oxidation in NP cells (Fig. 3d’’). Similarly, in the presence of glucose and glutamine, Glutor treated cells showed a decrease in average ECAR, whereas, glycolysis-dependent ECAR was only affected at higher Glutor concentration. Moreover, unlike control cells, Glutor treated cells in presence of oligomycin (ETC inhibition) were unable to increase ECAR (Fig. 3d’,d’’’). Noteworthy, presence of glutamine affected glucose-dependent ECAR in control cells i.e. glucose addition did not increase ECAR suggesting hindered glycolytic flux. These data imply that glutamine is not sufficient to rescue cell metabolism in the absence of glucose and in fact may interfere with glucose utilization by NP cells.

Considering that GLUT1/3 inhibition did not result in NP cells switching to glutamine oxidation, we investigated whether glucose restriction resulted in utilization of fatty acids to maintain TCA cycle flux. For these experiments, OCR was measured during endogenous conditions (no substrate), followed by the sequential addition of substrate (glucose + palmitate-

BSA), oligomycin, FCCP, and finally Etomoxir (CPT1 inhibitor; inhibits mitochondrial import of fatty acid) (Fig. 3e-e'''). Similar to measurements with glutamine, endogenous OCR was decreased in Glutor-treated cells (Fig. 3e'') and the addition of glucose + palmitate-BSA did not rescue OCR in Glutor-treated cells (Fig. 3e',e''). Moreover, inhibiting fatty acid import with ETO resulted in ~25% decrease in OCR in control cells and ~15-25% decrease in Glutor treated cells (Fig. 3e, e''). It was interesting to note that unlike glutamine, inclusion of BSA-palmitate with glucose did not interfere with ECAR induction in control cells. However, palmitate did not increase ECAR in Glutor treated cells, which remained significantly lower than control cells (Fig. 3e',e'''). Taken together, these metabolic experiments suggested that loss of GLUT1/3 function did not result in NP cells switching to glutamine or fatty acid oxidation and glucose import through GLUT1/3 is indispensable for their metabolism.

Nucleus pulposus-specific deletion of GLUT1 in skeletally mature mice does not affect disc health

To elucidate the role and test the apparent redundancy of GLUT1 seen in our *in vitro* experiments, we generated a conditional Glut1 knock-out in the mouse NP, driven by a tamoxifen-inducible $K19^{CreERT}$ allele (Fig. 4a). The $K19^{CreERT}$;$Glut1^{f/f}$ (cKO^{K19}) and littermate control $Glut1^{f/f}$ (WT) mice were injected at 3 months (3M) and collected at 9 months (9M). Robust *Glut1*/*Slc2a1* mRNA knockdown ~80-90% was confirmed by qRT-PCR (Fig. 4b). Deletion of GLUT1 protein was confirmed by fluorescence immunohistochemistry in both lumbar and caudal discs (Fig. 4c,c') and well as Western blot (Fig. 4d,d'; S.Fig. 2a,a''). These results validate the cKO^{K19} mouse model and confirm NP-specific deletion of GLUT1 protein expression in skeletally mature mice.

We also confirmed the expression of alternative glucose transporters and determined if their levels are affected in Glut1 cKO^{K19} mice. The mRNA levels of *Glut3* and *Glut9*, as well as sodium-glucose cotransporter *Sglt1* showed comparable levels between the WT and Glut1 cKO^{K19} mice (Fig. 4e-e''). Furthermore, in line with previous findings in human disc, Western blot confirmed that GLUT3 and GLUT9 protein levels remained robust in the NP of WT and cKO mice, with significantly lower abundance in the AF (Fig. 4f-g'; S.Fig. 2b-c'') [23]. Based on these findings, we hypothesized that baseline levels of alternative glucose transporters in the NP, including GLUT3, GLUT9, and SGLT1 may be sufficient to sustain glucose transport and preserve disc health in GLUT1-deficient mice.

Histological changes were assessed in lumbar and caudal discs of WT and Glut1 cKO^{K19} at 9M of age (Fig. 5a). Despite the robust expression of GLUT1 in the NP of healthy discs, Glut1 cKO^{K19} animals presented with no significant changes in the average grade of degeneration as measured by Modified Thompson Score (Fig. 5b) or in the distribution in grades of degeneration (Fig. 5b') in the NP of lumbar discs. There was a change in the distribution in grades of degeneration in the lumbar AF, however it did not indicate increased degeneration. Curiously, caudal Glut1 cKO^{K19} discs showed a slight decrease in the average grade of NP degeneration (Fig. 5b'') and distributions skewed towards lower grades of degeneration for NP and AF as well (Fig. 5b'''). Taken together, NP-specific deletion of GLUT1 in adult mice had few discernible effects on disc degeneration in lumbar or caudal discs.

To understand the impact of loss of GLUT1 on disc height (DH) and disc height index (DHI), µCT imaging was performed on 9M WT and Glut1 cKO^{K19} mice (Fig. 5c). In line with the histological analysis, we observed no changes in either DH or DHI in lumbar discs, however, there was a slight increase in both metrics in caudal discs (Fig. 5c'-c'''). The increased DHI in caudal discs could not be accounted for by changes in NP cell area (Fig. 5d) or in the aspect ratio of the NP tissue compartment (Fig. 5d').

To determine whether Glut1 cKO^{K19} show alterations in cell phenotypic makers and extracellular matrix (ECM) composition that does not reflect into grades of disc degeneration, we assessed the abundance of key extracellular matrix proteins in WT and Glut1 cKO^{K19} discs. Keratin-19 (K19), an NP cell phenotypic marker, showed no difference in abundance, suggesting the NP cell phenotype was maintained in Glut1 cKO^{K19} mice (Fig. 5e,e'). Interestingly, there was a significant decrease in the level of aggrecan – the major proteoglycan found in the NP – as well as chondroitin sulfate (CS) in the NP compartment of Glut1 cKO^{K19} mice (Fig. 5f,f',g,g'). To understand if the decrease in aggrecan and its predominant glycosaminoglycan (GAG) chain was due to aggrecan turnover, we quantified changes in a neoepitope marker of cleaved aggrecan, ARGxx. However, there was no difference in ARGxx levels in discs of WT and Glut1 cKO^{K19} mice suggesting possible decrease in synthesis of these molecules (Fig. 5h,h'). Overall, Glut1 cKO^{K19} mice showed only minor changes in NP ECM.

We also made note of the significant difference in the distribution of grades of degeneration in the AF compartment of both lumbar and caudal discs in Glut1 cKO^{K19} mice (Fig. 5b',b'''). To assess AF ECM, we analyzed collagen fiber architecture using Picrosirius Red staining coupled with polarized imaging (S.Fig. 3a, b). Under polarized light, green fluorescing

fibers are thin, yellow fluorescing fibers are intermediate, and red fluorescing fibers are thick. Our study finds that collagen fiber thickness is unaltered in lumbar AF (S.Fig. 3a', a''), however in Glut1 cKO^{K19} caudal discs, there was a significant increase in the percentage of thin (green) fibers and a decrease in thick (red) fibers (S.Fig. 3b, b''). This suggests that NP-specific deletion of GLUT1 may alter collagen fibers in the AF towards a thinner and more immature composition.

Loss of GLUT1 does not alter expression of genes involved in compensatory metabolic pathways

To understand if disc health in Glut1 cKO^{K19} mice is maintained by regulation of compensatory mechanisms, we analyzed the NP transcriptome using microarray. There was similar variance between the gene expression values in NP cells from WT and Glut1 cKO^{K19} mice, and the two phenotypes did not cluster independently along three principal components (S.Fig. 4a). When analyzed using a p-value cutoff of $p \leq 0.05$ and a fold-change of ±2, several differentially expressed genes emerged from the dataset (S.Fig. 4b,c), the most significant being *Slc2a1*, i.e. *Glut1*. However, PANTHER gene ontological analysis discovered no significantly enriched biological processes or molecular functions in the up- and down-regulated gene sets (data not shown). Furthermore, when the data were analyzed using more stringent parameters – FDR ≤ 0.05 and fold-change of ± 2 – the only differentially expressed gene was *Glut1*/*Slc2a1* (S.Fig. 4d).

The microarray analysis clearly shows that loss of GLUT1 causes strikingly few transcriptional changes in NP cells. This suggests that compensatory metabolic pathways do not require alterations in gene expression, despite the strict dependence of NP cells on glucose uptake. Changes in flux through alternative glucose transporters may therefore be sufficient to maintain glycolytic capacity in the NP of GLUT1 cKO mice.

GLUT1 expression in notochord/NP is not required for normal disc development

Considering that GLUT1 deletion in skeletally mature mice had no consequential effect on intervertebral disc health, we tested whether there was temporal dependency on GLUT1 function, specifically if it was required for normal embryonic and perinatal development of the NP. We crossed Glut1$^{f/f}$ mice with notochord and floorplate specific constitutive Foxa2^{Cre} mice to generate notochord/NP specific GLUT1 knockout mice - Foxa2^{Cre}; Glut1$^{f/f}$ (i.e. cKO^{Foxa2}) and littermate control (WT) mice (S.Fig.5a) were aged to postnatal day 7 (p7) and 14 weeks (14wk).

Immunohistochemistry confirmed a significant decrease in GLUT1 expression in the NP compartment of cKO^{Foxa2} mice at p7 (S.Fig. 5b, c) and 14wk (S.Fig. 5d, e). Despite the substantial GLUT1 knockdown (S.Fig. 5f), lumbar and caudal discs from cKO^{Foxa2} did not present with any of the criteria for degeneration – in fact all NP and AF compartments from p7 mice had a Modified Thompson Score of 1 (S.Fig. 5g, g', h, h'). At 14wk, the distribution in the grades of degeneration in cKO^{Foxa2} was different from the WT in lumbar NP and AF, as well as caudal NP, however the distributions favored lower grades of degeneration in the cKO^{Foxa2} mice (S.Fig. 5i, i'). Consequently, cKO^{Foxa2} mice lumbar AF had a slightly lower Modified Thompson Score, implying better morphological attributes, while lumbar NP and caudal NP and AF showed no significant difference from WT (S.Fig. 5 j, j'). These results suggest that glucose uptake through GLUT1 is not a critical player for the development and early maintenance of the NP.

DISCUSSION

The fact that loss of GLUT1 expression in the disc does not result in disc degeneration, transcriptomic changes, or metabolic disruption was baffling; especially considering the prominence of GLUT1 as a highly enriched NP phenotypic marker and the requirement for GLUT1 in the functional maintenance of other skeletal tissues including bone and cartilage [27,28,31]. Indeed, our study underscores that although glucose is the indispensable metabolite, it appears that GLUT1 is not singularly required to maintain glycolytic capacity, and therefore, is not necessary for NP cell survival. Conversely, we hypothesize that maintaining ATP levels through glycolysis and TCA metabolites is so vital for disc health and NP cell viability that the cells have inherently built-in redundancy to ensure uninterrupted supply of glucose through alternative glucose importers.

In the hypoxic niche of the intervertebral disc, NP cells primarily rely on glycolysis for bioenergetics and highly express GLUT1 which is considered one of their key phenotypic markers. We therefore investigated the role GLUT1 plays in NP cell metabolism by using two highly potent GLUT1 inhibitors [35,36]. Surprisingly, blocking GLUT1 in NP cells did not affect glucose uptake and bioenergetics suggesting an alternate mechanism for glucose import. In contrast, bone cells which primarily depend on glucose for their differentiation and maturation during development highly express GLUT1 which is responsible for 75% glucose uptake [27]. We and others have previously shown that NP cells express GLUT3 and GLUT9 [8,23]. Therefore, we delineated contribution of GLUT3 in NP cells using a dual GLUT1/3 inhibitor Glutor, which

revealed that 80-90% glucose was imported through these two carriers [39]. Importantly, unlike GLUT1 inhibition, Glutor treatment significantly inhibited glycolysis suggesting that GLUT3 is the critical high-capacity glucose importer in NP cells.

It is known that under nutrition constraints or increased metabolic demand cells undergo metabolic reprogramming for maintaining their function and survival [30,40,41]. When glucose uptake is blocked, primarily glycolytic proinflammatory macrophages and cancer cells switch their metabolism to alternative substrates such as glutamine and fatty acids [30,40]. Similarly, a very recent study showed that deletion of GLUT1 in articular and growth plate chondrocytes resulted in increased cellular glutamine oxidation for survival [31]. Similarly, osteoblasts are shown to shift to glutamine but not palmitate oxidation in absence of glucose, whereas, myoblasts prefer palmitate oxidation over glutamine oxidation [27]. It is important to note that NP cells exhibit metabolic plasticity. For example, when lactate export through MCT4 is inhibited in NP cells, the cells undergo an incomplete metabolic switch from glycolytic to oxidative metabolism fueled by pyruvate oxidation [16]. However, blocking lactate export still results in a 2-fold increase in the glycolytic intermediate, glucose-6-phosphate, implying glucose was still the major metabolite fueling pyruvate metabolism [16]. While NP cells do have the capacity to metabolize alternative energy sources, such as fatty acids through mitochondrial β-oxidation [8], many studies including ours show that glucose starvation leads to cell death [12,14,22]. Therefore, alternative energy sources such as glutamine, glycogen and fatty acids are not sufficient for compensating the loss of glucose import in NP cells. Further supporting this notion, we noted that NP cells did not shift to glutamine or palmitate oxidation when glucose import was impeded by GLUT1/3 inhibition. Rather, in contrast to other cell types, overall oxygen consumption rate significantly decreased underscoring the fact that glucose is the primary metabolic fuel for ATP generation through glycolysis and is critical for NP cell survival [8,39]. This also raised an interesting possibility that robust decrease in GLUT1 and GLUT3 levels may contribute to metabolic failure and massive cell death of NP cells seen in HIF-1α^{cKO} mice [9].

We have previously shown that in SM/J mice, a mouse model of early onset spontaneous degeneration, GLUT1 levels in NP decline and our data here indicate that levels are lower during aging, an important risk factor governing disc degeneration [33,42,43]. These findings were contradictory to our *in vitro* findings that showed minimal or no change in NP cell metabolism and their survival following GLUT1 inhibition. To clarify this seeming contradiction and to delineate whether loss of GLUT1 expression *in vivo* causes disc degeneration, we utilized two mouse

models, an inducible Glut1 cKO^{K19} and constitutive Glut1 cKO^{Foxa2} to determine a causal link between GLUT1 and intervertebral disc health. In the comparisons where there were significant differences in grade of degeneration, the GLUT1 cKO^{K19} mice rather showed slightly lower grades of degeneration. However, that is not to say that GLUT1 loss-of-function is protective in the disc, rather the discs are healthy in both WT and cKO animals. In an analogous study, we used a constitutive GLUT1 cKO model to determine if GLUT1 is involved in disc development and post-natal maturation. This hypothesis stems from the idea that GLUT1 may play a key role in the HIF-1α-dependent glycolytic metabolism in the developing embryonic NP [9]. Lack of apparent developmental defects in the discs from these mice further supported that NP cells are refractory to loss of GLUT1. Moreover, results suggest that avenues of compensation are available in the NP cells of these mice to allow them to survive deletion of an integral glycolytic component.

Our study finds that GLUT1 loss-of-function compensatory pathways do not involve transcriptional upregulation of other glucose transporters or metabolic enzymes. In fact, microarray analysis of NP from GLUT1 cKO^{K19} mice did not reveal a single differentially regulated transcript besides *Glut1/Slc2a1* when analyzed with an adjusted FDR p-value of 0.05. These data are corroborated by lack of changes in mRNA expression or protein levels of other *SLC2* family members and glucose importers expressed in the disc, namely GLUT3 and GLUT9 [23]. Importantly, however, glucose import may be maintained in NP cells by increased flux through these SLC2 transporters without concomitant increases in their expression levels. Furthermore, glucose may also enter the NP cell through sodium-glucose cotransport (SGLT) of which six isoforms have been identified [44]. SGLT is driven by the active extrusion of intracellular sodium, facilitating a concomitant import of extracellular glucose against plasma-membrane concentration gradients. Although SGLTs are attributed to glucose import across apical membranes, it is very possible they play a role in the NP compartment which is characterized by its high sodium concentrations and hyperosmolar niche. While the contribution of these transporters has not yet been studied in the context of the intervertebral disc, it is likely to be secondary to SLC2 family members.

Taken together, our study provides the first evidence of functional redundancy in GLUT transporters in a physiologically hypoxic NP compartment of the intervertebral disc and highlights its uniquely different niche than other skeletal tissue like articular and growth plate cartilage. Importantly, our findings underscore the importance of glucose as the indispensable metabolic fuel for NP cells and provides vital baseline for any cell-based therapies aimed at restoring the function of degenerating disc.

METHODS

Mice

All procedures regarding collection of animal tissues were performed as per approved protocols by the Institutional Animal Care and Use Committee (IACUC) of Thomas Jefferson University, in accordance with the IACUC's relevant guidelines and regulations. For postnatal deletion in NP compartment, *Glut1*$^{f/f}$ mice[45] were crossed with K19^{CreERT} mice (*Krt19*$^{tm1(cre/ERT)Ggu}$/J, Jackson Stock # 026925) to produce K19^{CreERT}; Glut1$^{f/f}$ (cKO^{K19}) mice, Glut1$^{f/f}$ littermate mice served as control (WT), and injected with three consecutive Tamoxifen at 3-months at a 100 μg/g.b.w.; these mice were collected 6-months post-recombination (9-months-old)[46]. For deletion of GLUT1 at embryonic time points, Glut1$^{f/f}$ mice were crossed with Foxa2^{Cre} mice to produce Foxa2^{Cre}; Glut1$^{f/f}$ (cKO^{FoxA2}) mice, littermate Foxa2^{Cre}; Glut1$^{f/+}$ and Glut1$^{f/f}$ mice served as control (WT); these mice were assessed at P7, 14-weeks. Foxa2^{Cre} allele drives robust expression specifically in the notochord and floorplate using combination of 5' notochord and 3' floorplate enhancers under the control of *Hspa1* promoter [47].

Immunofluorescence Microscopy and digital image analysis

7-μm thick mid-coronal disc sections were de-paraffinized and incubated in microwaved citrate buffer for 20 min or proteinase K for 10 min at room temperature, or Chondroitinase ABC for 30 min at 37 °C for antigen retrieval. Appropriate wildtype and cKO histological sections were blocked in 5% normal serum (Thermo Fisher Scientific, 10000 C) in PBS-T (0.4% Triton X-100 in PBS) and incubated with antibody against KRT19 (1:3, DSHB, TROMA-III/supernatant), CA3 (1:150, Santa Cruz, sc-50715), Aggrecan (1:50, Millipore, AB1031), GLUT-1 (1:200, Abcam, ab40084), ARGxx (1:200, Abcam, ab3773) and GLUT3 (1:200, Proteintech, 20403-1-AP) in blocking buffer at 4°C overnight. For GLUT-1 (1:200, Abcam, ab40084) and ARGxx (1:200, Abcam, ab3773) staining, Mouse on Mouse Kit (Vector laboratories, BMK2202) was used for blocking and primary antibody incubation. Tissue sections were thoroughly washed and incubated with Alexa Fluor®594 (Ex: 591 nm, Em: 614 nm) conjugated secondary antibody (Jackson ImmunoResearch Lab, Inc.), at a dilution of 1:700 for 1 h at room temperature in dark. The sections were washed again with PBS-T (0.4% Triton X-100 in PBS) and mounted with ProLong® Gold Antifade Mountant with DAPI (Thermo Fisher Scientific, P36934). All mounted slides were visualized with Axio Imager 2 (Carl Zeiss) using 5×/0.15 NAchroplan (Carl Zeiss), 10×/0.3 EC Plan-Neofluar (Carl Zeiss), or 20x/0.5 EC Plan-Neofluar (Carl Zeiss) objectives, X-Cite® 120Q Excitation Light Source (Excelitas), AxioCam MRm camera (Carl Zeiss), or LSM800

(Carl Zeiss) 20x/0.8 or 40x/1.3 Oil Plan-Apochromat (Carl Zeiss), AxioCam 506 mono (Carl Zeiss), and Zen2TM software (Carl Zeiss). DAPI-positive cells were analyzed to assess cell number in disc compartments. All quantifications were done in 8-bit greyscale using the Fiji package of ImageJ. Images were thresholded to create binary images, and NP and AF compartments were manually segmented using the Freehand Tool. These defined regions of interest were analyzed either using the Analyze Particles (cell number quantification) function or the Area Fraction measurement.

Protein extraction and Western Blotting

Following NP tissue extraction from Wildtype and GLUT1 cKO^{K19} mice, cells were washed on ice with ice-cold 1X PBS with protease inhibitor cocktail (Thermo Scientific). Cell were lysed with lysis buffer containing 1X protease inhibitor cocktail (Thermo Scientific), NaF (4 mM), Na3VO4 (20 mM), NaCl (150 mM), β- glycerophosphate (50 mM), and DTT (0.2 mM). Total protein was resolved on 10% SDS-polyacrylamide gels and transferred to PVDF membranes (Fisher Scientific). Membranes were blocked with 5% nonfat dry milk in TBST (50 mM Tris pH 7.6, 150 mM NaCl, 0.1% Tween 20) and incubated overnight at 4°C in 5% nonfat dry milk in TBST with anti-GLUT3 (1:500, Proteintech, 20403-1-AP) or anti-GLUT9 (1:500, Abcam, ab223470) antibodies. Specificity of all antibodies has been validated by the manufacturers using siRNA or negative control IgG. Immunolabeling was detected using ECL reagent and imaged using LAS4000 system (GE Life Sciences). Densitometric analysis was performed using ImageJ. All quantitative data is represented as mean ± SEM, n = 2-5 animal/genotype.

Isolation of NP cells, hypoxic culture, cell treatments

Rat NP cells were isolated as reported previously by Risbud and colleagues. Cells were maintained in Dulbecco's Modification of Eagle's Medium (DMEM) supplemented with 10% FBS and antibiotics. Cells were cultured in a Hypoxia Work Station (Invivo2 400, Ruskinn, UK) with a mixture of 1% O2, 5% CO2 and 94% N2. To investigate the effect of GLUT inhibition, NP cells were treated with 1) a cocktail of GLUT1 inhibitors (BAY-876, 10, 100 nM, Cayman, 19961) or (WZB-117, 1, 10 μM, Cayman, 19900) for 1 to 72 hours or 2) a GLUT1, 2 and 3 inhibitor (Glutor, 50, 100, and 250 nM, Sigma, SML2765) for 6 to 72 hours. Viability measurements following treatment of NP cells in hypoxia with BAY-876, WZB-117 and Glutor for 24-72 h were performed using a Calcein AM cell viability assay as per manufacturer's instructions (Invitrogen, C3100MP). All *in vitro* experiments were performed at least 3-6 independent times with 4 replicates/experiment/group and data represented as mean ± SEM.

Seahorse XF Analyzer Respiratory Assay

The oxygen ECAR and OCR were measured using method reported by Mookerjee and colleagues [37], briefly, rat NP cells were plated in 24-well Seahorse V7-PS assay plate and cultured for 36 hours in normoxia conditions. 24 h prior to assay cells were treated with GLUT1 inhibitors BAY-876 or WZB-117 and cultured under hypoxia. Prior to measurement cells were washed three times with 500 ul of KRPH (Krebs Ringer Phosphate HEPES) and incubated 37°C for 1 hour under 100% air. OCR and ECAR was measured by addition of 10 mM glucose, 2 µg oligomycin, 1 µM rotenone plus 1 µM myxothiazol. The rate of oxygen consumption and extracellular acidification were normalized to protein content of the appropriate well. For the substrate dependency assay, 24 h prior to assay, cells were treated with GLUT1/3 inhibitor Glutor and cultured under hypoxia. Prior to measurement cells were washed three times with 500 µl of KRPH (Krebs Ringer Phosphate HEPES) and incubated 37°C for 1 hour under 100% air. OCR and ECAR was measured by addition of 10 mM glucose plus 4mM glutamine, 2 µg oligomycin, 1 µM FCCP and 5 µM BPTES for glutamine oxidation. For fatty acid oxidation KRPH was supplemented with 0.5 mM L-carnitine and incubated 37°C for 1 hour under 100% air. OCR and ECAR was measured by addition of 10 mM glucose plus Palmitate-BSA (palmitate concentration 150 µM), 2 µg oligomycin, 1 µM FCCP and 5 µM Etomoxir. The rate of oxygen consumption and extracellular acidification were normalized to protein content of the appropriate well.

2-DG uptake assay

Rat NP cells (20,000 cells/well) were seeded in a 96 well plate in a complete medium and were grown for 48h in normoxia. After 48h cells were treated with glucose transporter inhibitors for 6 and 24 hours under hypoxia. The 2-DG uptake was measured following the (Abcam, ab136956) protocol. Briefly, adherent cells were washed three times with freshly prepared Krebs-Ringer-Phosphate-HEPES (KRPH) buffer (20mM HEPES, 5mM KH_2PO_4, 1mM $MgSO_4$, 1mM $CaCl_2$, 136mM NaCl, 4.7mM KCl, pH 7.4, 2% BSA). 2-DG (1µM) was added to the cells together with the respective inhibitors in KRPH buffer and incubated for 40 mins. DMSO and without 2-DG served as control. After 40 mins the 2-DG uptake was stopped by removing assay buffer and washing 3 times with ice-cold KRPH buffer. Cell lysis and endogenous NAD(P) degradation were performed by adding extraction buffer to the cells and incubated for 30 min at 85°C. Cell lysates were kept on ice for 5 min. and neutralization was performed by adding neutralization buffer. Then 2-DG uptake was measured following the protocol. All quantitative data are represented as mean ± SEM, n = 6 independent experiments, 4 replicates/experiment/group.

Real Time RT-PCR Analysis

NP tissue was micro-dissected from 9M Wildtype and Glut1 cKO^{K19} animals. Tissues from L1/2-L6/S1 and Ca1/2-Ca14/15 of same mouse were pooled and served as a single sample stored into RNAlater® Reagent (Invitrogen, Carlsbad, CA) for minimum 2 days at -80°C (n = 7 mice/genotype; 20 discs/animal). Samples were homogenized with a Pellet Pestle Motor (Sigma Aldrich, Z359971), and RNA was extracted using RNeasy® Mini kit (Qiagen). RNA was quantified on a Nanodrop ND-100 spectrophotometer (Thermo Fisher Scientific). Purified RNA was then converted to cDNA using EcoDry™ Premix (Clonetech). Gene specific primers (IDT, IN) and the template cDNA were added to Power SYBR Green master mix (Applied Biosystems). Primer sets were designed and by IDT, Inc. (S. Table 1). Quantification of expression was done by the StepOnePlus Realtime PCR system (Applied Biosystem) using ΔΔCT method and *Hprt* to normalize gene expression.

Mouse Histological analysis

Mouse spines were harvested and fixed in 4% PFA for 24-48 hours and decalcified in EDTA (12.5-20%) at 4°C for 15-21 days prior to paraffin embedding. Mid-coronal 7 μm disc sections (Ca5/6-Ca8/9, L1/2-L6/S1) were stained with Safranin O/Fast Green/Hematoxylin or Picrosirius red, then visualized using a light microscope (AxioImager 2, Carl Zeiss) or a polarizing microscope (Eclipse LV100 POL, Nikon). Histopathological grading was performed on n = 5 mice/genotype with 6 discs per mouse (30 discs/genotype) at P7 and 14 weeks (WT and Glut1cKO^{Foxa2}); n = 8 mice/genotype with 6 discs per mouse (48 discs/genotype) at 9 months (WT and Glut1cKO^{K19}). Modified Thompson grading was used to score NP and AF compartments by 3 blinded graders. Aspect ratio of NP was determined by width divided by height of the NP tissue measured from Safranin O/Fast Green staining images of mid-coronal tissue sections from 9 month-old WT and Glut1cKO^{K19} animals, n = 6 mice/genotype with 3 discs per mouse (18 discs/genotype) using ImageJ software (http://rsb.info.nih.gov/ij/).

Micro-CT analysis

Micro-CT (μCT) scans (Bruker, Skyscan 1275) were performed on WT and Glut1cKO^{K19} spines fixed with 4% PFA. Lumbar spine segments incorporating L2-S1 (7 mice/genotype) were scanned with an energy of 50 kV at 200 μA, resulting in 15 μm^3 voxel size resolution. Intervertebral disc height and the vertebral length were measured and averaged along the dorsal, midline, and ventral regions in the sagittal plane and Disc height index (DHI) was calculated as previously described [42].

Transcriptomic Analysis and Enriched Pathways

RNA was quantified on a Nanodrop ND-100 spectrophotometer, followed by RNA quality assessment analysis on an Agilent 2200 TapeStation (Agilent Technologies, Palo Alto, CA). Fragmented biotin labeled cDNA (from 100 ng of RNA) was synthesized using the GeneChip WT Plus kit according to ABI protocol (Thermo Fisher Scientific). Gene chips, Mouse Clariom S were hybridized with 2.5 µg fragmented and biotin-labeled cDNA in 100 µl of hybridization cocktail. Arrays were washed and stained with GeneChip hybridization wash & stain kit using Gene chip Fluidic Station 450. Chips were scanned on an Affymetrix Gene Chip Scanner 3000 7G, using Command Console Software. Quality Control of the experiment was performed by Expression Console Software v 1.4.1. Chp files were generated by sst-rma normalization from Affymetrix .cel file using Expression Console Software. Experimental group was compared with control group by using Transcriptome array console 4.0 and DEGs with a Fold Change ±2, p-value or FDR<0.05. PANTHER tool was used to compute enriched pathways in DEGs that are altered with a Fold Change ±2, p-value <0.05. For evaluating highly expressed genes in the developing notochord/NP and NP of healthy adult mice, data deposited by Peck *et al.* GSE100934[32] and Novais *et al.* GSE134955[33] were used.

Statistical analysis

Quantitative data are presented as mean ± SEM and data distribution was checked with Shapiro-Wilk normality test, and unpaired t-test or Mann-Whitney test was used as appropriate. Comparisons between more than 2 groups were performed by the one-way ANOVA or Kruskal-Wallis test with appropriate post-hoc analyses (Dunn's or Dunnett's or Sidak's multiple comparisons test) using Prism9 (Graphpad Software); $p<0.05$. For histopathological analysis showing percent-degenerated-discs and Picrosirius red percentage AF area, $\chi 2$ test was used.

Data Availability

All data generated or analyzed during this study are included in this published article (and its Supplementary files) or deposited on the GEO database (GSE208396).

Acknowledgements: This work is supported by grants from the National Institutes of Health R01 AR055655, R01 AR073349, R01 AR074813 (MVR) and T32 AR052273 (IMS). We acknowledge Drs. E. Dale Abel for proving GLUT1$^{f/f}$ mice, Ernestina Schipani for FoxA2^{Cre}; HIF-1$\alpha^{f/f}$ mice and Michael Kuehn for FoxA2^{Cre}.

Authors Contributions: ESS, SNJ, MVR, IMS designed the project. SNJ, VM, and ESS performed all experiments. ESS, SNJ, VM, IMS and MVR wrote and edited the manuscript.

Disclosures: The authors declare that they have no conflicts of interest or disclosures with the contents of this article.

REFERENCES

1. Silagi, E. S., Schipani, E., Shapiro, I. M. & Risbud, M. V. The role of HIF proteins in maintaining the metabolic health of the intervertebral disc. *Nat. Rev. Rheumatol.* **17**, 426–439 (2021).
2. Tessier, S., Madhu, V., Johnson, Z. I., Shapiro, I. M. & Risbud, M. V. NFAT5/TonEBP controls early acquisition of notochord phenotypic markers, collagen composition, and sonic hedgehog signaling during mouse intervertebral disc embryogenesis. *Dev. Biol.* **455**, 369–381 (2019).
3. Risbud, M. V. *et al.* Defining the phenotype of young healthy nucleus pulposus cells: Recommendations of the spine research interest group at the 2014 annual ORS meeting. *J. Orthop. Res.* **33**, 283–293 (2015).
4. Rajpurohit, R., Risbud, M., Ducheyne, P., Vresilovic, E. & Shapiro, I. Phenotypic characteristics of the nucleus pulposus: expression of hypoxia inducing factor-1, glucose transporter-1 and MMP-2. *Cell Tissue Res.* **308**, 401–407 (2002).
5. Risbud, M. V. *et al.* Nucleus pulposus cells express HIF-1 alpha under normoxic culture conditions: a metabolic adaptation to the intervertebral disc microenvironment. *J. Cell. Biochem.* **98**, 152–159 (2006).
6. Fujita, N., Chiba, K., Shapiro, I. M. & Risbud, M. V. HIF-1alpha and HIF-2alpha degradation is differentially regulated in nucleus pulposus cells of the intervertebral disc. *J Bone Min. Res* **27**, 401–412 (2012).
7. Madhu, V. *et al.* Hypoxic Regulation of Mitochondrial Metabolism and Mitophagy in Nucleus Pulposus Cells Is Dependent on HIF-1α–BNIP3 Axis. *J. Bone Miner. Res.* (2020) doi:10.1002/jbmr.4019.
8. Agrawal, A. *et al.* Normoxic stabilization of HIF-1alpha drives glycolytic metabolism and regulates aggrecan gene expression in nucleus pulposus cells of the rat intervertebral disk. *Am. J. Physiol. Cell Physiol.* **293**, C621–C631 (2007).
9. Merceron, C. *et al.* Loss of HIF-1alpha in the notochord results in cell death and complete disappearance of the nucleus pulposus. *PLoS One* **9**, e110768 (2014).
10. Schoepflin, Z. R., Silagi, E. S., Shapiro, I. M. & Risbud, M. V. PHD3 is a transcriptional coactivator of HIF-1a in nucleus pulposus cells independent of the PKM2-JMJD5 axis. *FASEB J.* **31**, (2017).
11. Grunhagen, T., Shirazi-Adl, A., Fairbank, J. C. T. & Urban, J. P. G. Intervertebral Disk Nutrition: A Review of Factors Influencing Concentrations of Nutrients and Metabolites. *Orthop. Clin. North Am.* **42**, 465–477 (2011).
12. Bibby, S. R. S. & Urban, J. P. G. Effect of nutrient deprivation on the viability of intervertebral disc cells. *Eur. Spine J.* **13**, 695–701 (2004).
13. Naqvi, S. M. & Buckley, C. T. Extracellular matrix production by nucleus pulposus and bone marrow stem cells in response to altered oxygen and glucose microenvironments. *J. Anat.* (2015) doi:10.1111/joa.12305.
14. Guehring, T. *et al.* Notochordal intervertebral disc cells: sensitivity to nutrient deprivation. *Arthritis Rheum.* **60**, 1026–34 (2009).
15. Hartman, R. *et al.* Age-dependent changes in intervertebral disc cell mitochondria and bioenergetics. *Eur. Cells Mater.* **36**, 171–183 (2018).
16. Silagi, E. S. *et al.* Lactate Efflux From Intervertebral Disc Cells Is Required for Maintenance of Spine Health. *J. Bone Miner. Res.* **35**, 550–570 (2020).
17. Wang, D. *et al.* Lactate oxidative phosphorylation by annulus fibrosus cells: evidence for lactate-dependent metabolic symbiosis in intervertebral discs. *Arthritis Res. Ther.* **23**, (2021).
18. Ashinsky, B. G. *et al.* Intervertebral Disc Degeneration Is Associated With Aberrant Endplate Remodeling and Reduced Small Molecule Transport. *J. Bone Miner. Res.* **35**,

1572–1581 (2020).
19. Silagi, E. S. *et al.* Bicarbonate Recycling by HIF-1–Dependent Carbonic Anhydrase Isoforms 9 and 12 Is Critical in Maintaining Intracellular pH and Viability of Nucleus Pulposus Cells. *J. Bone Miner. Res.* **33**, 338–355 (2018).
20. Wang, C., Gonzales, S., Levene, H., Gu, W. & Huang, C. Y. C. Energy metabolism of intervertebral disc under mechanical loading. *J. Orthop. Res.* **31**, 1733–8 (2013).
21. Bartels, E. M., Fairbank, J. C., Winlove, C. P. & Urban, J. P. Oxygen and lactate concentrations measured in vivo in the intervertebral discs of patients with scoliosis and back pain. *Spine (Phila. Pa. 1976).* **23**, 1–7; discussion 8 (1998).
22. Bibby, S. R. S., Jones, D. a, Ripley, R. M. & Urban, J. P. G. Metabolism of the intervertebral disc: effects of low levels of oxygen, glucose, and pH on rates of energy metabolism of bovine nucleus pulposus cells. *Spine (Phila. Pa. 1976).* **30**, 487–496 (2005).
23. Richardson, S. M., Knowles, R., Tyler, J., Mobasheri, A. & Hoyland, J. A. Expression of glucose transporters GLUT-1, GLUT-3, GLUT-9 and HIF-1alpha in normal and degenerate human intervertebral disc. *Histochem. Cell Biol.* **129**, 503–11 (2008).
24. Heilig, C. *et al.* Implications of glucose transporter protein type 1 (GLUT1)-haplodeficiency in embryonic stem cells for their survival in response to hypoxic stress. *Am. J. Pathol.* **163**, 1873–1885 (2003).
25. Wang, D. *et al.* A mouse model for Glut-1 haploinsufficiency. *Hum. Mol. Genet.* (2006) doi:10.1093/hmg/ddl032.
26. Swarup, A. *et al.* Modulating GLUT1 expression in retinal pigment epithelium decreases glucose levels in the retina: impact on photoreceptors and Müller glial cells. *Am. J. Physiol. Cell Physiol.* **316**, C121–C133 (2019).
27. Wei, J. *et al.* Glucose Uptake and Runx2 Synergize to Orchestrate Osteoblast Differentiation and Bone Formation. *Cell* **161**, 1576–1591 (2015).
28. Lee, S. Y., Abel, E. D. & Long, F. Glucose metabolism induced by Bmp signaling is essential for murine skeletal development. *Nat. Commun.* **9**, 4831 (2018).
29. Swarup, A. *et al.* Deletion of GLUT1 in mouse lens epithelium leads to cataract formation. *Exp. Eye Res.* **172**, 45–53 (2018).
30. Freemerman, A. J. *et al.* Myeloid Slc2a1-Deficient Murine Model Revealed Macrophage Activation and Metabolic Phenotype Are Fueled by GLUT1. *J. Immunol.* **202**, 1265–1286 (2019).
31. Wang, C. *et al.* Deletion of Glut1 in early postnatal cartilage reprograms chondrocytes toward enhanced glutamine oxidation. *Bone Res.* **9**, (2021).
32. Peck, S. H. *et al.* Whole Transcriptome Analysis of Notochord-Derived Cells during Embryonic Formation of the Nucleus Pulposus. *Sci. Rep.* **7**, (2017).
33. Novais, E. J. *et al.* Comparison of inbred mouse strains shows diverse phenotypic outcomes of intervertebral disc aging. *Aging Cell* **19**, 213148 (2020).
34. Silagi, E. S., Batista, P., Shapiro, I. M. & Risbud, M. V. Expression of Carbonic Anhydrase III, a Nucleus Pulposus Phenotypic Marker, is Hypoxia-responsive and Confers Protection from Oxidative Stress-induced Cell Death. *Sci. Rep.* **8**, 4856 (2018).
35. Wu, Q. *et al.* GLUT1 inhibition blocks growth of RB1-positive triple negative breast cancer. *Nat. Commun.* **11**, (2020).
36. Liu, Y. *et al.* A small-molecule inhibitor of glucose transporter 1 downregulates glycolysis, induces cell-cycle arrest, and inhibits cancer cell growth in vitro and in vivo. *Mol. Cancer Ther.* **11**, 1672–1682 (2012).
37. Mookerjee, S. A., Gerencser, A. A., Nicholls, D. G. & Brand, M. D. Quantifying intracellular rates of glycolytic and oxidative ATP production and consumption using extracellular flux measurements. *J. Biol. Chem.* **292**, 7189–7207 (2017).
38. Martínez-Reyes, I. & Chandel, N. S. Mitochondrial TCA cycle metabolites control

physiology and disease. *Nat. Commun.* **11**, (2020).
39. Reckzeh, E. S. *et al.* Inhibition of Glucose Transporters and Glutaminase Synergistically Impairs Tumor Cell Growth. *Cell Chem. Biol.* **26**, 1214-1228.e25 (2019).
40. Brooks Robey, R. *et al.* Metabolic reprogramming and dysregulated metabolism: cause, consequence and/or enabler of environmental carcinogenesis? *Carcinogenesis* **36 Suppl 1**, S203–S231 (2015).
41. Ito, K. & Suda, T. Metabolic requirements for the maintenance of self-renewing stem cells. *Nat. Rev. Mol. Cell Biol.* **15**, 243–256 (2014).
42. Choi, H. *et al.* A novel mouse model of intervertebral disc degeneration shows altered cell fate and matrix homeostasis. *Matrix Biol.* **70**, 102–122 (2018).
43. Ohnishi, T. *et al.* Caspase-3 knockout inhibits intervertebral disc degeneration related to injury but accelerates degeneration related to aging. *Sci. Rep.* **9**, (2019).
44. Allison, S. Structures of sodium-glucose cotransporters. *Nat. Rev. Nephrol.* **18**, 137 (2022).
45. Winkler, E. A. *et al.* GLUT1 reductions exacerbate Alzheimer's disease vasculo-neuronal dysfunction and degeneration. *Nat. Neurosci.* **18**, 521–530 (2015).
46. Mohanty, S., Pinelli, R. & Dahia, C. L. Characterization of Krt19 CreERT allele for targeting the nucleus pulposus cells in the postnatal mouse intervertebral disc. *J. Cell. Physiol.* **235**, 128–140 (2020).
47. Uetzmann, L., Burtscher, I. & Lickert, H. A mouse line expressing Foxa2-driven Cre recombinase in node, notochord, floorplate, and endoderm. *Genesis* **46**, 515–522 (2008).

FIGURE LEGENDS

Figure 1. GLUT1, an enriched NP marker is a HIF-1 target and its expression declines with aging. (a) Graph showing top genes expressed in mouse NP cells at E12.5, P0 and 6-months (GSEs: GSE100934 and GSE134955). (b) Schematic showing deletion of HIF-1α exon 2 to generate mutant HIF-1α mRNA. (b') Representative IHC images of NP cell phenotypic markers GLUT1 and CA3 in HIF-1α WT and HIF-1α^{cKO} (Foxa2^{Cre}; HIF-1$\alpha^{f/f}$) mice (scale bar = 50 µm). (c-c') Representative images and quantification of GLUT1 in BL6/J mice with aging (scale bar = 25 µm) (n = 5 mice/timepoint; 3-6 discs/animal; 15-30 discs/timepoint). (d) Western blot showing GLUT1 levels in mouse NP with aging (n = 2 mice/timepoint; 20 discs/animal were pooled). (e-e') Effect of short term (1 hour) GLUT1 inhibition by BAY-876 on ECAR and OCR measurements in NP cells. (f-f') Effect of short term GLUT1 inhibition by WZB-117 on ECAR and OCR measurements in NP cells. (g) Short term GLUT1 inhibition by BAY-876 and WZB-117 results in decreased average ECAR. (h) Short term GLUT1 inhibition does not affect total OCR in BAY-876 and WZB-117 treated cells. (h') Mitochondrial OCR measurements following short term treatment by BAY-876 and WZB-117. (n = 6 independent experiments, 4 technical replicates/experiment/group). Quantitative measurements represent mean ± SEM. Significance was determined using an one-way ANOVA (g-h') or Kruskal Wallis (c') with Dunnett's or Dunn's post hoc test as appropriate.

Figure 2. Long-term inhibition of GLUT1 does not affect glycolytic or oxidative metabolism in NP cells. (a-a') ECAR and OCR profiles following long term GLUT1 inhibition (24 h) by BAY-876 in NP cells. (b-b') ECAR and OCR profiles following long term GLUT1 inhibition (24 h) by WZB-117. (c-d) Long term GLUT1 inhibition by BAY-876 and WZB-117 did not alter (c) ECAR and (d) OCR measurements. (e-e') Long term GLUT1 inhibition by (e) BAY-876 and (e') WZB-117 did not affect ATP production by NP cells. Quantitative measurements represent mean ± SEM (n = 4 biological replicates, 4 technical replicates/experiment/group). Significance was determined using one-way ANOVA.

Figure 3. GLUT3 facilitates uptake of glucose, a metabolic substrate indispensable for NP cells. (a-a') 2-DG uptake in cells treated with GLUT1 inhibitors and GLUT1/3 dual inhibitor Glutor from (a) 6 to (a') 24 hours. (b-b") Cell viability following GLUT1 (BAY-876 and WZB-117) and GLUT1/3 inhibition (Glutor). (c) Representative image of GLUT3 staining in HIF-1$\alpha^{f/f}$ (WT) and HIF-1α^{cKO} (Foxa2^{Cre}; HIF-1$\alpha^{f/f}$) mice (scale bar = 100 µm). PO: primary center of

ossification, HC: hypertrophic chondrocytes (d-d') OCR and ECAR traces in Glutor treated and control cells in presence of Glutamine, and BPTES (d'') quantification of endogenous, basal, maximal, and glutamine dependent OCR derived from traces shown in d, and (d''') glutamine-dependent average ECAR and glycolysis derived from traces in d'. (e-e') OCR and ECAR traces in Glutor treated and control NP cells in presence of Palmitate-BSA, and ETO and (e'') quantification of endogenous, basal, maximal, glutamine dependent OCR from traces in e, and (e''') average ECAR and glycolysis derived from traces shown in e'. Quantitative measurements represent mean ± SEM (n = 4-6 biological replicates, 4 technical replicates/experiment/group). Significance of differences was determined using one-way ANOVA with Sidak's or Dunnett's post hoc test as appropriate.

Figure 4. Conditional deletion of Glut1 in NP compartment of adult mice. (a) Schematic showing $K19^{Cre}$ mediated deletion of *Glut1/Slc2a1* exon 3-8 to generate NP specific *Glut1* mutant. (b) quantification of *Glut1* in $Glut1cKO^{K19}$ mice (n = 7 mice/genotype; 20 discs/animal). (c-c') Representative IHC images and quantification of GLUT1 in 9-month-old WT and $Glut1cKO^{K19}$ (scale bar = 200 µm and 50 µm) (n = 8 WT, 7 cKO mice; 6 lumbar and 3 caudal discs/animal). (d-d') Western Blot and quantification of GLUT1 levels in NP of WT and $Glut1cKO^{K19}$ mice (n = 5 mice/genotype; 20 discs/animal). White dotted lines demarcate disc compartments. (e-e'') qRT-PCR of *Glut3*, *Glut9*, *Sglt1* in WT and $Glut1cKO^{K19}$ mice (n = 7 mice/genotype; 20 disc/animal). (f,f') Western blot and quantification of GLUT3 and (g,g') GLUT9 (n = 5 mice/genotype; 20 disc/animal). Quantitative measurements represent mean ± SEM, significance of differences was determined using Mann-Whitney test.

Figure 5. $Glut1cKO^{K19}$ mice do not show adverse effects on intervertebral disc health. (a) Representative SafraninO/FastGreen images of 9-month-old WT and $Glut1cKO^{K19}$ lumbar and caudal discs (scale bar = 200 µm). (b-b''') Modified Thompson Scores of NP and AF compartments in WT and $Glut1cKO^{K19}$ lumbar and caudal discs. (n = 7 mice/genotype; 3-4 lumbar and 2-3 caudal discs/animal, 25-27 lumbar and 20-21 caudal discs/genotype) (c) Representative µCT images of lumbar and caudal motion segments (scale bar = 1 mm). (c'-c'') Quantification of lumbar and caudal DHI, DH, and VBH. (n = 7 animals/genotype; Vertebrae L3-6, Ca5-6, and Discs L3/4-L6/S1, Ca5/6-7/8 per animal). (d-d') Quantification of NP cell number and aspect ratio from lumbar and caudal discs. (n = 7 mice/genotype; 1-4 lumbar discs/animal, 2-3 caudal discs/animal; 25-27 lumbar and 20-21 caudal discs/genotype). (e-h') Representative IHC and quantification of keratin-19 (K19), aggrecan (Acan), ARGxx, and chondroitin sulfate

(CS) (scale bar = 200 μm, ARGxx scale bar = 100 μm). (n = 7 mice/genotype; 1-3 caudal discs/animal; 15-20 caudal discs/genotype). White dotted lines demarcate disc compartments. Significance for grading distribution was determined using a χ^2 test. Significance of differences was determined using an unpaired t-test (c', c''', d, d', e') or Mann-Whitney test (b, b', c'-c''',d', f' g', h'), as appropriate. Quantitative measurements represent mean ± SEM.

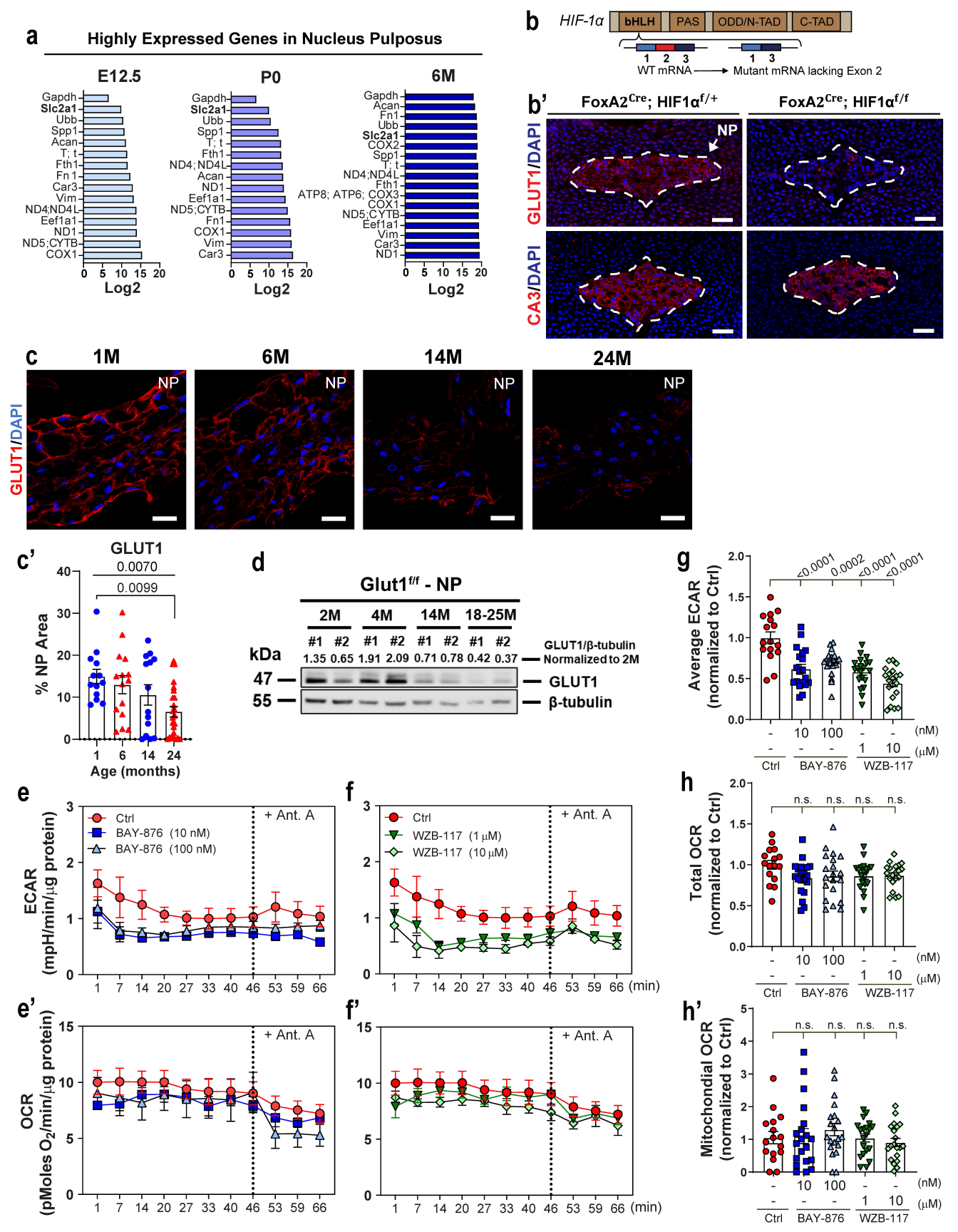
a
Highly Expressed Genes in Nucleus Pulposus
E12.5
P0
6M
Gapdh
Slc2a1
Ubb
Spp1
Acan
T; t
Fth1
Fn1
Car3
Vim
ND4;ND4L
Eef1a1
ND1
ND5;CYTB
COX1
COX2
ATP8; ATP6; COX3
Log2
b
HIF-1α
bHLH
PAS
ODD/N-TAD
C-TAD
WT mRNA
Mutant mRNA lacking Exon 2
b'
FoxA2Cre; HIF1αf/+
FoxA2Cre; HIF1αf/f
GLUT1/DAPI
CA3/DAPI
NP
c
1M
6M
14M
24M
GLUT1/DAPI
c'
GLUT1
0.0070
0.0099
% NP Area
Age (months)
d
Glut1f/f - NP
2M
4M
14M
18-25M
kDa
1.35 0.65 1.91 2.09 0.71 0.78 0.42 0.37
GLUT1/β-tubulin Normalized to 2M
47
55
GLUT1
β-tubulin
e
ECAR (mpH/min/μg protein)
Ctrl
BAY-876 (10 nM)
BAY-876 (100 nM)
+ Ant. A
f
WZB-117 (1 μM)
WZB-117 (10 μM)
(min)
e'
OCR (pMoles O2/min/μg protein)
f'
g
Average ECAR (normalized to Ctrl)
<0.0001
0.0002
<0.0001
<0.0001
(nM)
(μM)
Ctrl
BAY-876
WZB-117
h
Total OCR (normalized to Ctrl)
n.s.
h'
Mitochondial OCR (normalized to Ctrl)

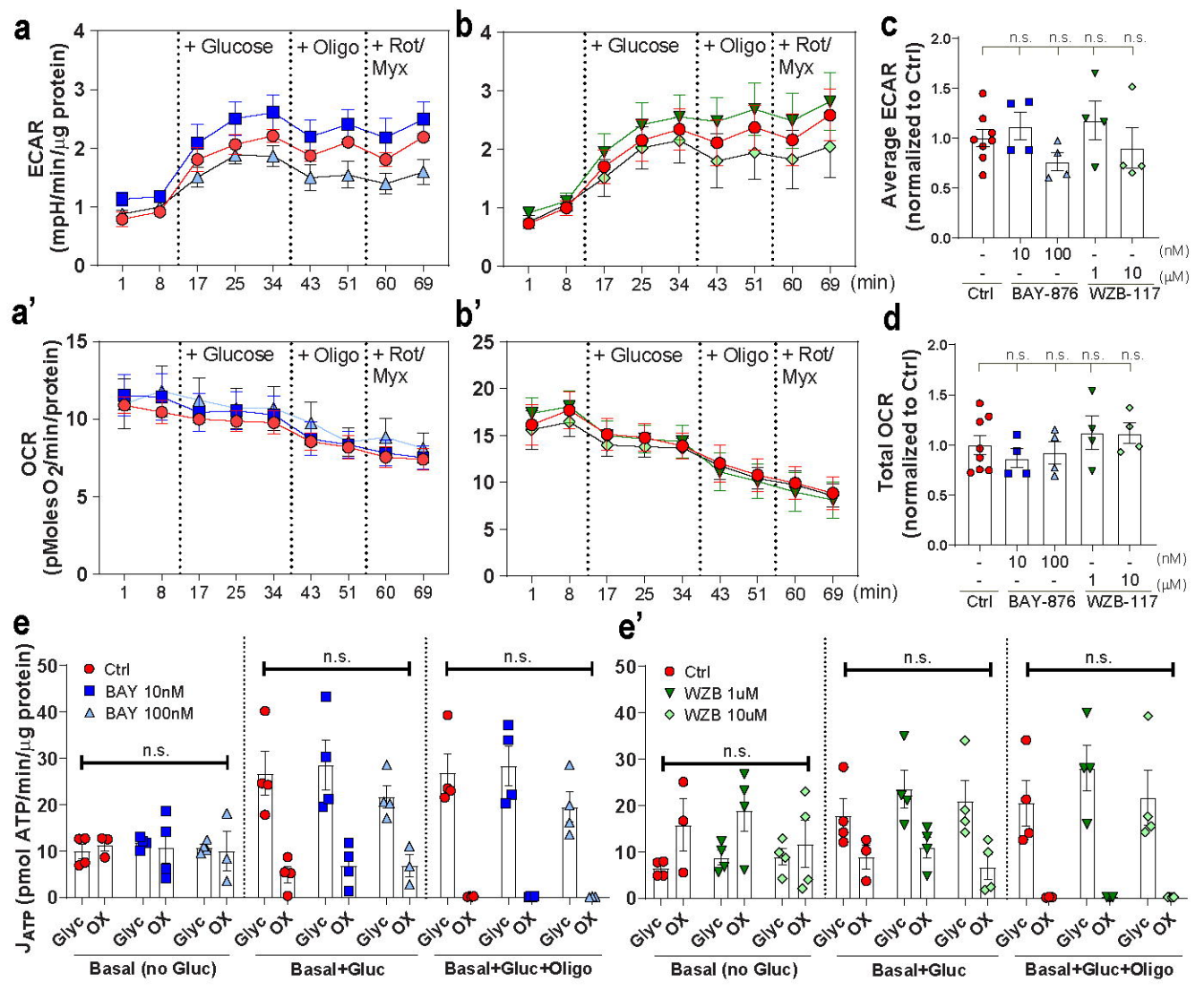
a
ECAR (mpH/min/µg protein)
+ Glucose
+ Oligo
+ Rot/ Myx
b
(min)
c
Average ECAR (normalized to Ctrl)
n.s.
(nM)
(µM)
Ctrl
BAY-876
WZB-117
a'
OCR (pMoles O2/min/protein)
b'
d
Total OCR (normalized to Ctrl)
e
Ctrl
BAY 10nM
BAY 100nM
JATP (pmol ATP/min/µg protein)
Glyc
OX
Basal (no Gluc)
Basal+Gluc
Basal+Gluc+Oligo
e'
WZB 1uM
WZB 10uM

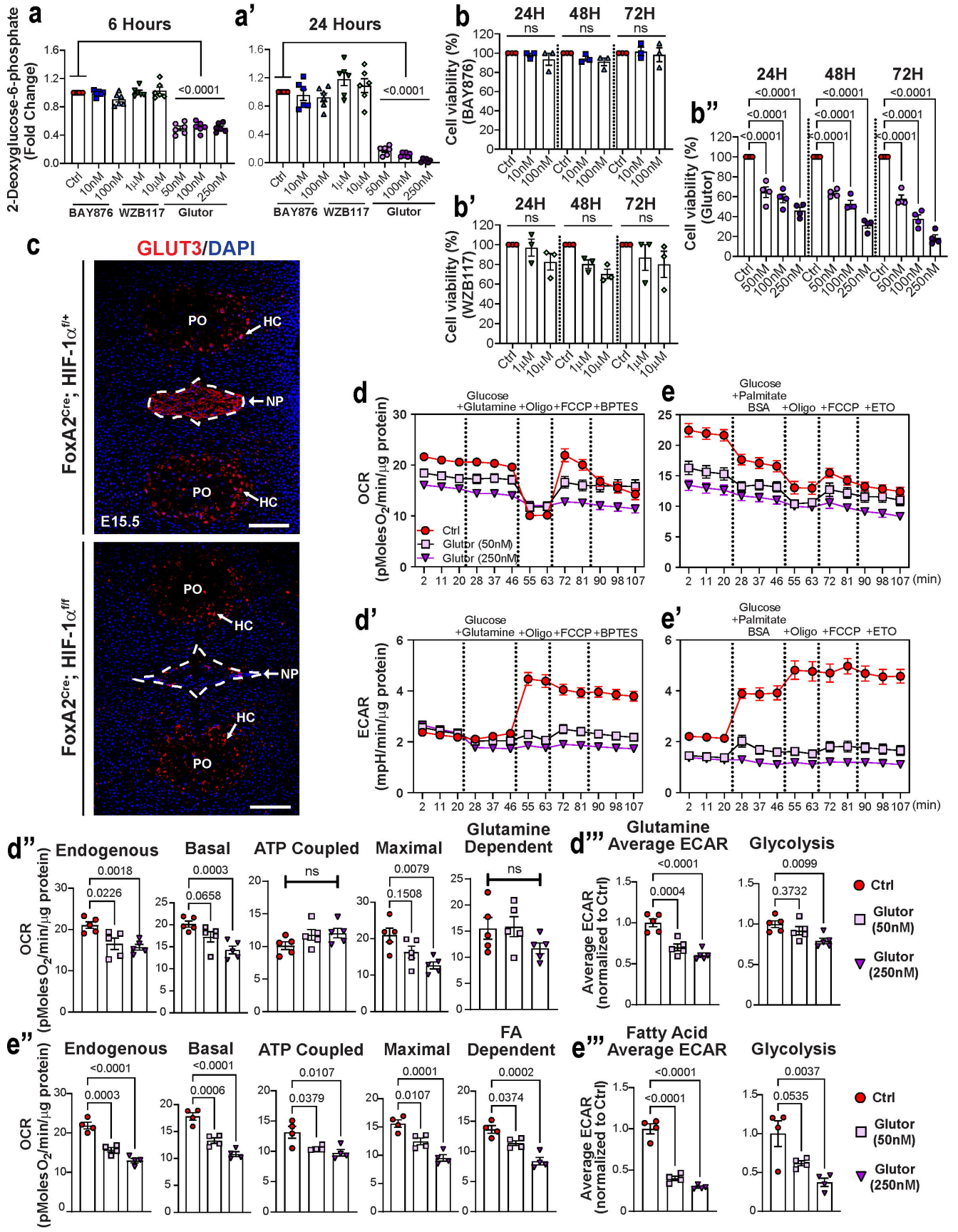
a
6 Hours
a'
24 Hours
2-Deoxyglucose-6-phosphate (Fold Change)
<0.0001
Ctrl
10nM
100nM
1μM
10μM
50nM
100nM
250nM
BAY876
WZB117
Glutor
b
24H
48H
72H
ns
Cell viability (%) (BAY876)
b'
Cell viability (%) (WZB117)
b''
Cell viability (%) (Glutor)
c
GLUT3/DAPI
FoxA2Cre; HIF-1αf/+
FoxA2Cre; HIF-1αf/f
PO
HC
NP
E15.5
d
Glucose
+Glutamine
+Oligo
+FCCP
+BPTES
OCR (pMoles O2/min/μg protein)
Ctrl
Glutor (50nM)
Glutor (250nM)
e
+Palmitate
BSA
+ETO
(min)
d'
ECAR (mpH/min/μg protein)
e'
d''
Endogenous
Basal
ATP Coupled
Maximal
Glutamine Dependent
0.0018
0.0226
0.0003
0.0658
0.0079
0.1508
d'''
Glutamine Average ECAR
Glycolysis
Average ECAR (normalized to Ctrl)
0.0004
0.0099
0.3732
e''
FA Dependent
0.0003
0.0006
0.0107
0.0379
0.0001
0.0002
0.0374
e'''
Fatty Acid Average ECAR
0.0037
0.0535

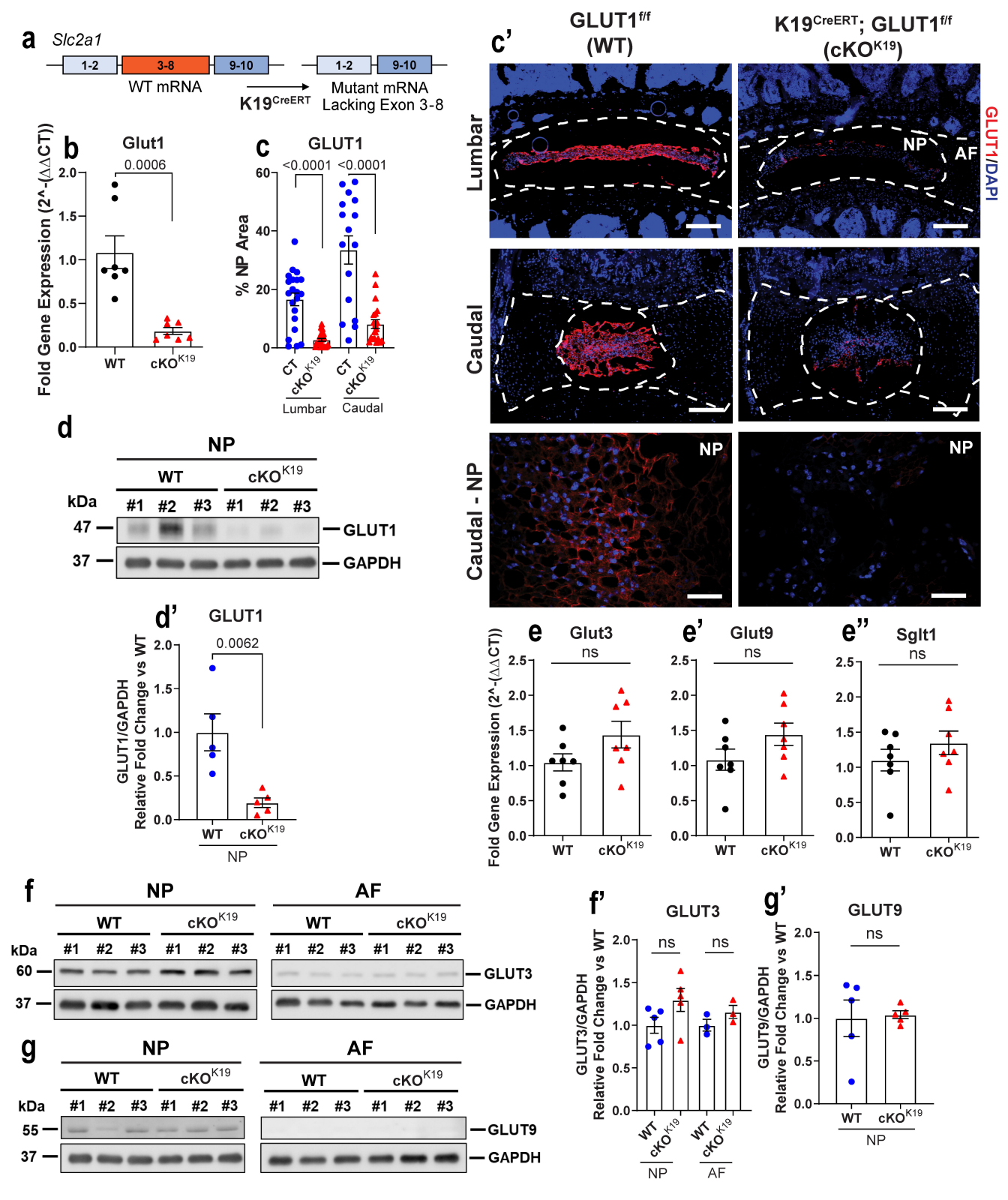
a
Slc2a1
1-2
3-8
9-10
WT mRNA
K19CreERT
1-2
9-10
Mutant mRNA
Lacking Exon 3-8
b
Glut1
0.0006
Fold Gene Expression (2^-(ΔΔCT))
WT
cKOK19
c
GLUT1
<0.0001
<0.0001
% NP Area
CT
cKOK19
CT
cKOK19
Lumbar
Caudal
c'
GLUT1f/f
(WT)
K19CreERT; GLUT1f/f
(cKOK19)
Lumbar
Caudal
Caudal - NP
NP
AF
GLUT1/DAPI
d
NP
WT
cKOK19
kDa
#1 #2 #3 #1 #2 #3
47
37
GLUT1
GAPDH
d'
GLUT1
0.0062
GLUT1/GAPDH
Relative Fold Change vs WT
WT
cKOK19
NP
e
Glut3
ns
e'
Glut9
ns
e''
Sglt1
ns
Fold Gene Expression (2^-(ΔΔCT))
WT
cKOK19
f
NP
AF
WT
cKOK19
kDa
#1 #2 #3 #1 #2 #3
60
37
GLUT3
GAPDH
f'
GLUT3
ns
ns
GLUT3/GAPDH
Relative Fold Change vs WT
WT
cKOK19
NP
AF
g
NP
AF
WT
cKOK19
kDa
#1 #2 #3 #1 #2 #3
55
37
GLUT9
GAPDH
g'
GLUT9
ns
GLUT9/GAPDH
Relative Fold Change vs WT
WT
cKOK19
NP

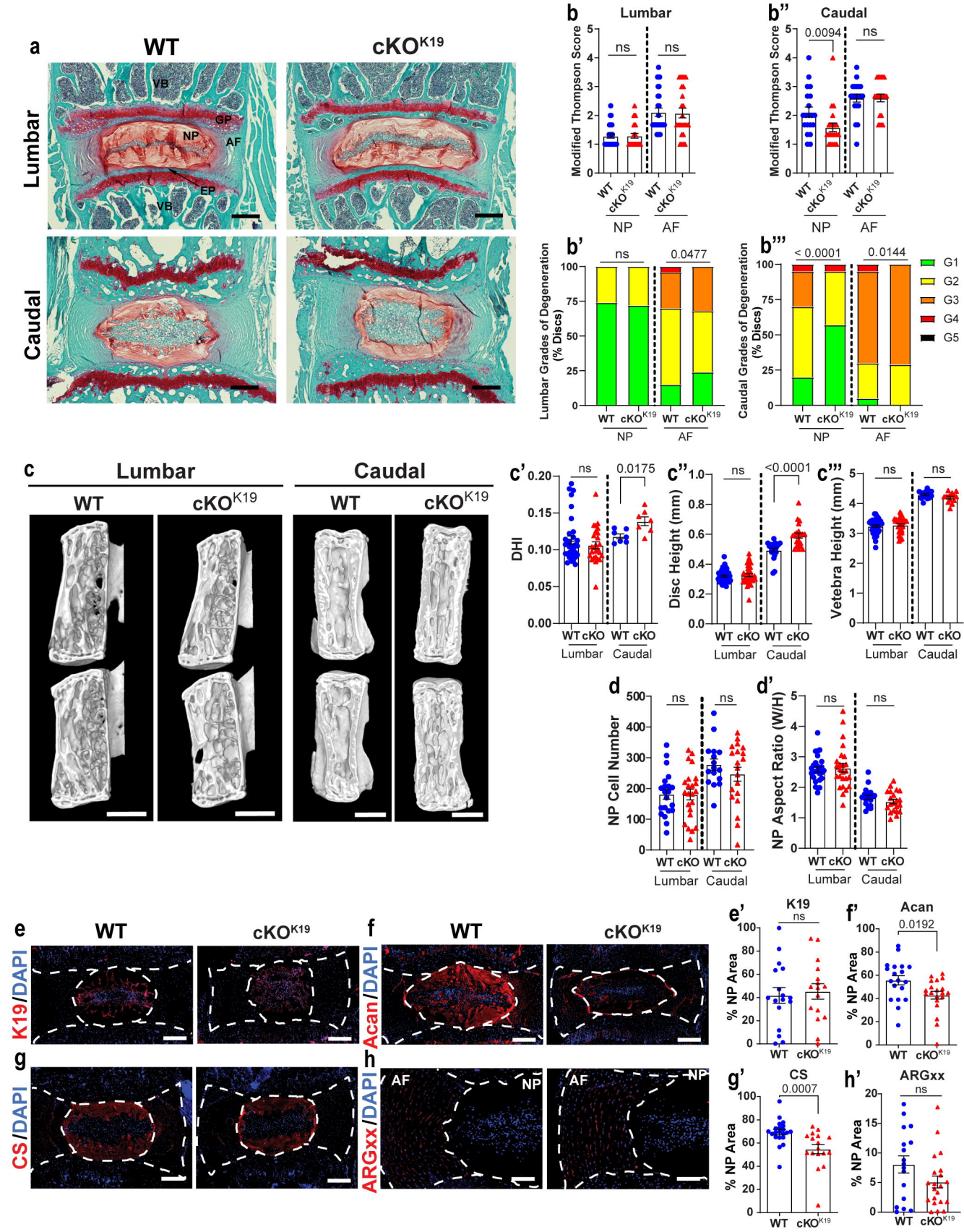
a
WT
cKO^K19
Lumbar
Caudal
VB
GP
NP
AF
EP
VB
b
Lumbar
Modified Thompson Score
ns
ns
WT
cKO^K19
NP
AF
b''
Caudal
0.0094
ns
b'
0.0477
Lumbar Grades of Degeneration (% Discs)
b'''
< 0.0001
0.0144
Caudal Grades of Degeneration (% Discs)
G1
G2
G3
G4
G5
c
Lumbar
Caudal
c'
DHI
0.0175
c''
Disc Height (mm)
<0.0001
c'''
Vetebra Height (mm)
WT cKO
Lumbar
Caudal
d
NP Cell Number
d'
NP Aspect Ratio (W/H)
e
K19/DAPI
f
Acan/DAPI
g
CS/DAPI
h
ARGxx/DAPI
AF
NP
e'
K19
% NP Area
f'
Acan
0.0192
g'
CS
0.0007
h'
ARGxx